Eur. Phys. J. B (2012) 85: 291
DOI: 10.1140/epjb/e2012-30276-x

THE EUROPEAN PHYSICAL JOURNAL B

Regular Article

Controlling fast electron transfer at the nano-scale by solitonic excitations along crystallographic axes

A.P. Chetverikov[1,2], W. Ebeling[1,3,a], and M.G. Velarde[1,4]

[1] Instituto Pluridisciplinar, Universidad Complutense, Paseo Juan XXIII, 1, 28040 Madrid, Spain
[2] Dept. of Physics, Saratov State University, Astrakhanskaya 83, 410012 Saratov, Russia
[3] Institut für Physik, Humboldt-Universität Berlin, Newtonstrasse 15, 12489 Berlin, Germany
[4] Fundacion Universidad Alfonso X El Sabio, Villanueva de la Canada, 28691 Madrid, Spain

Received 31 March 2012 / Received in final form 8 May 2012
Published online 29 August 2012 –

Abstract. We present computational evidence of the possibility of fast, supersonic or subsonic, nearly loss-free transport of electrons bound to lattice solitons along crystallographic axes in two-dimensional anharmonic crystal lattices.

1 Introduction

In the present work we discuss the problem of control of electrons by acoustic lattice soliton excitations, a form of electron *surfing*, which may have different origin such as e.g. mechanical or electrical shocks generated by contacts of the tip of an electron field microscope with a suitable anharmonic crystal lattice layer. We consider systems of a few hundred atoms on a plane interacting with one or a few added, excess electrons. The quantum dynamics of those electrons is described by kinetic equations (Pauli approximation) [1,2] what restricts our approach to moderately albeit high enough temperatures where coherent phases do not play a significant role. Earlier we have already discussed the interaction between electrons and strongly localized lattice excitations of soliton-type in one- (1d) and two-dimensional (2d) lattices [3–5]. For the electron dynamics we used the tight-binding approximation (TBA) and for the lattice particles a classical Hamiltonian albeit with the quantum Morse interactions [6]. As a result of this mixed anharmonic classical-quantum TBA dynamics we could show that the electrons "like" to follow the trajectories of soliton-like excitations. In the 1d case we have predicted several interesting phenomena, in particular the "vacuum-cleaner" effect, i.e., the electron probability density is gathered by solitons which along their trajectory act as long range correlators [7,8]. Noteworthy is that these excitations move in general with *supersonic* velocity, v_s, or velocities a bit below the sound velocity depending on the parameter values, on the initial conditions and on the electron-lattice interaction [9,10]. This means that electrons bound to lattice solitons (in short called solectrons) can move with quite high velocities of more than 1000 m/s in a solid medium, faster than the drift velocities of "free" electrons, which usually do not exceed 1–100 cm/s.

Let us consider the *anharmonic* lattice with an added, excess electron with charge e hopping from site to site along the lattice. The electron interacts with the initially neutral lattice atoms, shifts their energy levels and locally induces electric polarization in neighboring lattice sites. This is like an *attractive* interaction, therefore the electron tends to seat on such locally compressed regions of the lattice. This is the Landau selftrappping or polaron idea [11–14]. In 1d we can assume that the shift of the energy of an atom at site n is given by

$$E_n = E_n^0 - \frac{1}{2}\chi[q_{n+1} - q_{n-1}], \tag{1}$$

where the $q_{n\pm1}$ denote the spatial displacements of the nearest-neighbors. In the 2d case we can assume that the energy shifts are proportional to the polarization field strength. For large enough distances between atom and electron r the polarization potential has the asymptotic form $\alpha_e e^2/\epsilon_0 r^4$, with α_e the electric polarizability of the atom and ϵ_0 the dielectric constant of the medium. Let us assume now that the electron is located at the position $\mathbf{r}$ and that the lattice atoms are located at the positions $= \mathbf{r}_j$ with $j = 1, 2, \ldots N$. For example, in the case of hydrogen a bound state is found in the singlet channel, with binding energy 0.754 eV. Because of the Pauli principle, no bound state is observed in the spin triplet state. The energy of induced polarization of an atom is

$$\frac{\alpha_e}{2}\mathbf{E}(\mathbf{r}_n)^2. \tag{2}$$

Note that $\alpha_e = (9/2)a_B^2$ for hydrogen atoms and about the same order or even higher for other types of atoms. According to this expression, an electron located at the

[a] e-mail: werner_ebeling@web.de

origin generates together with an atom number j at the place $\mathbf{r_j}$ the polarization energy [5,15]

$$U_j(r_j) = -U_e \left[\frac{h^4}{(r_j^2 + h^2)^2} \right], \tag{3}$$

where h defines the characteristic cut-off distance of polarization interactions which may span a few atomic diameters ($h > a_B$ where a_B is the Bohr radius). The maximal polarization energy, U_e, depends on the polarization constant of the atom,

$$U_e = \frac{\alpha_e e^2}{2\epsilon_0^2 h^4}. \tag{4}$$

For our computer simulations we truncate the polarization potential at the cut-off distance $r = 1.5\sigma$ (more on this further below; σ is the equilibrium interatomic lattice distance) and hence we set

$$U_e(r_j) = -U_e \left[\frac{h^4}{(r_j^2 + h^2)^2} - \frac{h^4}{(r_0^2 + h^2)^2} \right], \tag{5}$$

$$U(r_j) = 0 \qquad \text{if} \qquad r_j > r_0 \qquad r_0 = 1.5\sigma. \tag{6}$$

The overall electrical potential generated by all the atoms on an electron placed at $\mathbf{r}$ is then given by

$$U(\mathbf{r}) = \sum_j U_j(\mathbf{r} - \mathbf{r}_j), \tag{7}$$

where we see the interaction with the lattice units. Clearly, any cluster of atoms may generate a potential hole or trap where the electron density might be concentrated. Any displacement of the atoms changes the polarization energy and the electron will try to follow these changes. This is the basic "slaving" ingredient leading to the polaron (harmonic case) [11,12] and to the solectron formation (anharmonic case) [13,14].

In the 2d-case we will use a simple generalization of (1) based on the mean-field assumption that the energy levels are shifted linearly with the mean polarization field. This assumption is acceptable, if the amplitude of the polarization fields is large in comparison to the oscillation energies around the potential minima $\hbar\omega$. In the TBA the energy levels E_n are functions of the atomic configuration, given by the coordinates $\{\mathbf{r}_1, \ldots, \mathbf{r}_N\}$. Assuming that the original atomic binding energy E_0 eigenvalues are shifted like the polarization potential we get

$$E_n \simeq E_0 + \sum_j \delta U_j(\mathbf{r}_n - \mathbf{r}_j). \tag{8}$$

Consequently, the energies E_n form a rapidly evolving landscape that is determined by the actual atom lattice positions.

Let us estimate the effects of local lattice compressions on the transition probabilities. The probability of hopping between neighboring atoms i and j depends on the relative distance between atoms r in an exponential way

$$W_{\text{hop}}(i,j) \simeq \exp[-2\alpha_h r]. \tag{9}$$

This follows from the fact that transitions are based on the overlap of wave functions. In other words hopping along the lattice, the electron moves faster in the compressed parts.

Our idea of controlling electrons is to generate a traveling pathway with locally compressed atoms, such that an electron will form bound states with the local lattice distortion, eventually being trapped and suitably guided at our will. This is to be added to the Landau-Pekar polaron, where it is the moving electron that locally perturbs a neighborhood of lattice atoms thus being self-trapped. In the parameter range we shall consider here the latter effect is assumed to weaker than the former. Thus the solectron formation is controlled by two atomic constants α_e and α_h determining polarization and hopping effects, respectively. The constant α_h is determined by the size of the atoms and may be of the order of $0.5/\sigma$. Accordingly, transitions beyond more than two atomic diameters are very unlikely to occur. Adding thermal effects to account for moderate temperatures, the lattice atoms with Morse interactions will be in the weakly nonlinear regime of oscillations [16], which can be treated by classical Langevin equations. For visualizations, the atomic core electrons are in a first approximation represented by Gaussian densities, thus permitting to follow the underlying lattice compressions shown by the excess density above initial equilibrium level due to the overlapping of the Gaussian peaks.

After introducing in Section 2 the model for the description of 2d-lattices and solitons, we discuss in section 3 the stochastic evolution of the added, free electrons by Pauli-type master equations, which allows us to follow the motion of solectrons in the lattice. We also discuss several examples of controlling the electron path in the lattice by the excitation of solectrons. This way we show the possibility to transfer electrons along one of the three crystallographic axes in e.g. a triangular lattice over quite long distances with negligible spreading of the electron probability densities. Finally in Section 4 we summarize our findings and comment on the possible connection with old and recent experiments on PDA polymer crystal layers and electron surfing mediated by surface acoustic waves (SAW) in piezoelectric GaAs layers.

2 Lattice dynamics, initial conditions and methods of visualization of excitations

The Hamiltonian of our 2d lattice consists of a classical lattice component H_a, and the contribution of the electrons H_e, which includes the interactions with the lattice deformations. For the lattice part, the Hamiltonian is

$$H_a = \frac{m}{2} \sum_k v_k^2 + \frac{1}{2} \sum_{k,j} V(r_k,\, r_j) - \sum_k \frac{\alpha_e}{2} \mathbf{E}(\mathbf{r}_k)^2. \tag{10}$$

The subscripts locate the atoms all with equal mass, m, at lattice sites and the summations run from 1 to N. For later convenience we introduce here a term which takes into account the polarizability of the atoms α_e in an external field $\mathbf{E}(\mathbf{r_k})$. We have in mind a strong local field as created e.g. by the tip of a field emission microscope. We shall assume that the lattice units repel each other with exponentially repulsive forces and attract each other with weak dispersion forces. As earlier said the characteristic length determining the repulsion between the particles in the lattice is σ. We limit ourselves to nearest-neighbors only using the relative distance $r = |r_n - r_k|$. The above conditions are met by the Morse potential [6]. Thus we set

$$V(r) = D\left\{\exp[-2b(r-\sigma)] - 2\exp[-b(r-\sigma)]\right\}. \quad (11)$$

By imposing the cutoff of the potential at 1.5σ, we exclude unphysical cumulative interaction effects arising from the influence of lattice units outside the first neighborhood of each atom [3,4]. To study, at varying temperature, the nonlinear excitations of the lattice and the possible electron transport in a lattice in the simplest approximation it is sufficient to know the coordinates of the lattice (point) particles at each time and the interaction of lattice deformations with electrons. Coordinates of particles are obtained by solving the equations of motion of each particle under the influence of all possible forces. The latter shall also include friction and random forces accounting for a Langevin model bath in the heated lattice. For convenience in the 2d lattice dynamics rather than using r, we use complex coordinates $Z = x + iy$, where x and y are Cartesian coordinates. Then the initial classical Newton deterministic equations corresponding to the lattice Hamiltonian (10) yields to a Langevin dynamics for the lattice units

$$\frac{d^2 Z_i}{dt^2} = \sum_k F_{ik}(Z_{ik}) z_{ik} + \left[-\gamma \frac{dZ_i}{dt} + \sqrt{2D_v}\,(\xi_{ix} + i\xi_{iy})\right], \quad (12)$$

where again an index i identifies a particle among all N particles of the ensemble, γ is a friction coefficient, D_v defines the intensity of stochastic forces, $\xi_{ix,y}$ denotes statistically independent generators of the Gaussian noise. $T = mD_v/\gamma$ (Einstein's relation). $Z_{ik} = Z_i - Z_k$ and $z_{ik} = (Z_i - Z_k)/|Z_i - Z_k|$ is the unit vector defining the direction of the interaction force F_{ik}, corresponding to the Morse potential, between the ith and the kth atoms in the lattice. To have dimensionless variables we consider the spatial coordinates rescaled with σ as unit length. Time is normalized to the inverse frequency of linear oscillations near the minimum of the Morse potential well, ω_M^{-1}, whereas energy is scaled with $2D$, where D is its depth as shown in (11). Further the stiffness parameter b (made dimensionless) defines the strength of the repulsion between atoms. The interaction force F_{nk} is given by

$$F_{ik} = F_{ik}(|Z_{ik}|) = -\frac{dV(r)}{dr}|_{r=|Z_{ik}|}. \quad (13)$$

In view of the above only those lattice units with coordinates Z_k, satisfying the condition $|Z_i - Z_k| < 1.5$, are taken into account in the sum in equation (12). In computer simulations the interaction of lattice units is considered to take place inside a rectangular cell $L_x \times L_y$ with periodic boundary conditions and depending on the symmetry of an initial distribution of units and their number N. For illustration = we consider a distribution corresponding to the minimum of potential energy for an equilibrium state of a *triangular* lattice $10\sigma \times 10(\sqrt{3}/2)\sigma$ for $N = 100$ or $20\sigma \times 20(\sqrt{3} = /2)\sigma$ for $N = 400$.

As the repulsion part of the Toda interaction is about the same as in the Morse case, in order to create lattice deformations leading to lattice solitons one can assume initially a compression and velocity profile corresponding to the analytical form of a 1d Toda soliton [17–20] in a given lattice row. The other lattice units remain at their equilibrium positions on a triangular lattice at zero temperature = [21,22]. As shown by Remoissenet [23], a broad spectrum of initial excitations, as e.g. excitations of rectangular profiles of are able to create solitons or cnoidal waves. For this reason we have experimented here with a broad range of initial conditions. For example we gave initially a suitable high momentum to one lattice site in the direction of one of the crystallographic axes in such a way that a successful start of a soliton was observed. This way we found that not only Toda profiles but also simpler initial conditions as pushing initially just one particle may be sufficient to create a soliton due to the "efficiency" of the Morse repulsion. For instance using the Toda profile along x, one of the six crystallographic directions in the triangular lattice, we can set

$$x_{n+1} - x_n = \sigma - \frac{1}{b_{eff}} \ln\left[1 + \frac{\sinh^2(\kappa)}{\cosh^2(\kappa n)}\right] \simeq \sigma - \frac{1}{b_{eff}} \frac{\sinh^2(\kappa)}{\cosh^2(\kappa n)}, \quad (14)$$

with the corresponding velocities and $x_1 = 0$. Here $b_{eff} = b$ is the dimensionless stiffness and κ is defined by the energy of the soliton. Another choice could be $b_{eff} = 1.5b$ which in fact provides much longer life and better robustness of the excited soliton.

For visualization and tracking the atomic electron densities we modeled the atoms as little spheres with "core" electrons represented by a Gaussian distribution centered at each lattice site:

$$\rho(Z,t) = \sum_{|Z - Z_i(t)| < 1.5\sigma} \exp\left[-\frac{|Z - Z_i(t)|^2}{2\lambda^2}\right]. \quad (15)$$

Using data about trajectories of particles $Z_n(t)$ and their velocities we can calculate the lattice atom distribution $\rho(Z,t)$. In Figure 1 we show a track of the running excitation (in "bubble chamber representation") which was created by pushing just one atom in the direction of the crystallographic axis x. We show the space and time evolution of the initial soliton density peak for the time interval $\Delta t = 3$ (measured in units of $1/\omega_M$, as earlier said). The parameter values of the potential are $b\sigma = 4$, $\lambda = 0.3\sigma$. The Langevin source corresponds to a rather low temperature, $T = 0.001$ (in dimensionless units). This corresponds

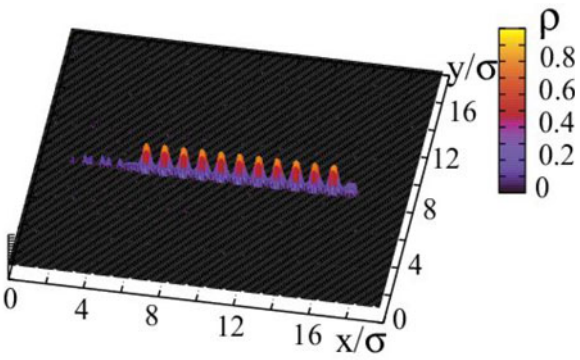

Fig. 1. (Color online) Triangular Morse lattice. The density of the core electrons of lattice atoms in the course of time. A soliton is excited by a strong pulse velocity $2v_s$ imposed to one lattice particle located not far from the left border (site 4, row 10) along and a rather high energy $2mv_0^2$ to the 4th atom in the row. A track of the excitation (in "bubble chamber representation") of the running soliton density is represented for the time interval $\Delta t = 3$ (measured in units of $1/\omega_M$) in a cumulative sequence as time proceeds. (Parameter values: $N = 400$, $b\sigma = 4$, $\lambda = 0.3\sigma$, and $T = 0.001$.)

to the mean kinetic energy of a particle $\langle T_{kin}\rangle$ reaching the value T. The soliton is moving along a crystallographic axis and was excited by a strong pulse of velocity $2v_0$ imposed at $t = 0$ to the 4th atom $n = 4$ in the 10th row with rather high energy $2mv_0^2$. The high-energetic soliton excited this way is quite long lasting in its motion along the chosen crystallographic axis. Transverse excitations and thermal collisions due to the source term in the Langevin equation do not play a significant role in the interval of observation (3 time units). From the length of the cumulative path and the time interval we may estimate the velocity. It appears that this strong local compression moves with velocity about $1.2v_{sound}$ with a lifetime of at least several time units. In the 2d triangular Morse lattice v_{sound} is slightly above 1 in our units. These features point to soliton-like behavior as for the 1d lattice [24]. Indeed, they move a few picoseconds with nearly unaltered profile and just this robustness is the reason that we can identify them with the proposed visualization method. Losses due to scattering and radiation of linear waves are quite low, due to the nearly integrable character of the problem. Note that the 2d solitons observed here, are similar to the so-called lump solutions of the Kadomtsev-Petiashvili equations [25]. We note further that including thermal effects due to our moderate temperatures, the lattice atoms are moving still in the weakly nonlinear regime [16].

In the following section we will show that the nanosize of our 2d-structure makes possible the existence of electric structures due to the interactions of the electrons with the nonlinear lattice deformations, similar to those seen in the 1d-case. We underline, that we cannot expect to see similar electric structures at large scales, due to screening of the charges.

3 Dynamics of electrons embedded into the 2d lattice and soliton-mediated effects

Let us now focus on the role played by one or several non-interacting electrons embedded into the atomic lattice, maybe as a result of doping or injection. Following Davydov [26], in 1d the deformation density created by a supersonic lattice soliton along a coordinate z in direction of the propagation can be approximated by

$$\rho_d(z,t) \simeq \rho_0 \mathrm{sech}^2(\kappa\xi), \qquad \xi = (z(t) - z(0) - v_s t)/\sigma, \quad (16)$$

where $z(t) = z(0) \pm v_s t$ is the actual position of the soliton at time t, v_s the (supersonic) soliton velocity and κ the reciprocal width of the soliton, which, in the strongly supersonic case, is proportional to the soliton velocity. Extending this formula to a 2d system, the z-coordinate has to be oriented along one of the crystallographic axes. The electronic bound states may be analytically calculated in the continuum (long-wave) approximation [26,27]. The ground state in the well created by the deformation density is bell-shaped and given by

$$\Phi_0(z,t) \simeq C\mathrm{sech}(\kappa\xi'), \qquad \xi' = (z(t) - z(0) - v_{se}t)/\sigma, \quad (17)$$

where v_{se} is the velocity of the electron bound to the lattice soliton, i.e., the solectron velocity. In the case that v_s is only slightly above the sound velocity, the solectron velocity is generally lower than the soliton velocity and may be even below the sound velocity [3,4,27]. The solectron density is the square of the wave function and has therefore the same shape as the soliton deformation which is a continuum version of the Toda soliton (see Eq. (14)). The corresponding density in the momentum space is the square of the Fourier transform ($p_z = \hbar k_z$). It is centered around the solectron momentum $p_{se} = m_{se}v_{se}$ where m_{se} is the effective mass of the solectron [26]. The ground state probability density in momentum space is in first approximation a Gaussian

$$P_0(p_z,t) \simeq C \exp\left[-\frac{(p_z \pm p_{se})^2}{(\hbar\kappa/\sigma)^2}\right]. \quad (18)$$

This is a *local* maximum near to the soliton momentum $\pm p_{se}$. The bound state energy increases for strongly supersonic solectrons with the square of the soliton velocity [26]. For appropriate parameter values, this estimate of the energy could possibly reach the order of 0.1–1.0 eV, what seems to be a rather high value relative to other known electronic binding energies. In earlier computer simulations with 1d Morse lattices [3–5] we observed solectrons in a temperature window of 0.1–1 D. Assuming potential wells of order 0.1–0.5 eV, the solectron ground state appears in the range 0.01–0.1 eV. This justifies the robustness or stability of the supersonic solectrons against thermal perturbations.

In order to study the evolution of the quantum states of the additional electrons interacting with the atoms in

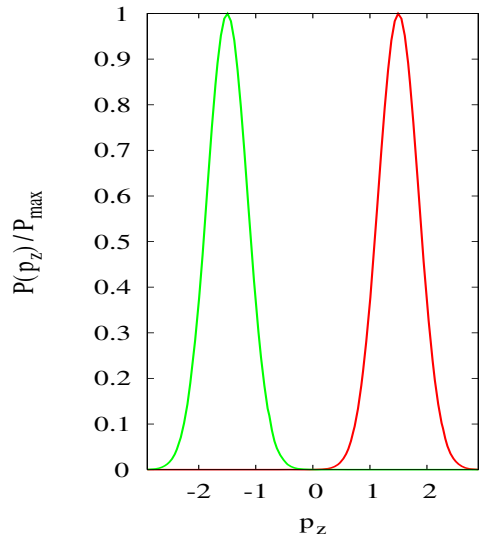

Fig. 2. (Color online) Density of the solectron bound state in momentum space for the cases of right- and left-running solectrons (schematic representation with $\kappa = 1$ and $p_{se} = 1.5$).

the 2d-lattice, we set [28]

$$H_{\rm el} = \sum_n E_n c_n^+ c_n + \sum_{n,n',m} t_{n,n',m}(\mathbf{r}_{n'} - \mathbf{r}_n) c_{n',m}^+ c_{n,m}, \tag{19}$$

with the transition matrix

$$t_{n,n',m} = \langle n', m | H_0 + V_{ea} | n, m \rangle. \tag{20}$$

Here n, m denote the internal quantum numbers of the states of electrons bound to the corresponding atoms at sites $\mathbf{r}_n$ and $\mathbf{r}_m$. The additional electrons can be in a localized, bound state, but they can also form extended states when they are excited above the edge of continuum. In the following we will assume for simplicity, that there is only one internal quantum state per atom and we will drop the internal quantum number m. If necessary, the internal state that characterizes the orbit as well as spin, can be included in the quantum number n. To further simplify the problem, the feedback of the electron distribution on the lattice dynamics (polaron-like effect) is neglected here. We set

$$H_e = \sum_n E_n c_n^+ c_n + \sum_{n,n'} t_{n,n'} c_{n'}^+ c_n. \tag{21}$$

The energy levels E_n may be approximated by the expressions given above (5)–(8). Then assuming that the original atomic binding energy E_0 eigenvalues are shifted like the polarization potential we get explicitely

$$E_n \simeq E_0 - \sum_{n'=1}^{N} \frac{U_e h^4}{[(\mathbf{r}_n - \mathbf{r}_{n'})^2 + h^2]^2}, \tag{22}$$

recalling that n denotes the internal quantum number of the electron state that is bound to the atom at site $\mathbf{R}_n$.

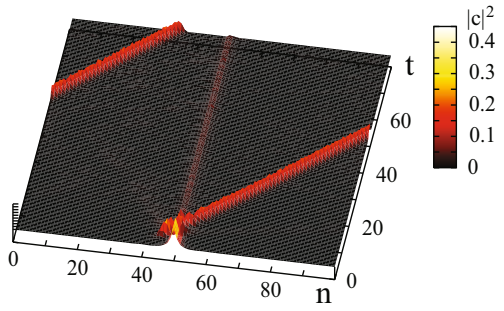

Fig. 3. (Color online) 1d Morse lattice. The added free electron probability density is carried with supersonic velocity along the path of an excited soliton initially at lattice site $n = 40$. The free electron is initially distributed in a Gaussian profile located near to a small potential well ($\epsilon = -15D$) at site $n = 50$. After about 8–10 time units the electron is catched by the moving potential well created by the soliton thus forming a solectron which moves supersonically but around 5 percent slower than the initial soliton, taken alone.

As a consequence, the energies E_n form a rather complex and rapidly changing landscape that is determined by the atomic positions $\{\mathbf{r}_1, \ldots, \mathbf{r}_N\}$.

The transition matrix elements $t_{n,n'}$ also depend on the atomic distances, $t_{n,n'} = t(\mathbf{r}_{n'} - \mathbf{r}_n)$. Following Slater [29] we take

$$t_{n,n'} = V_0 \exp[-\alpha_h |\mathbf{r}_n - \mathbf{r}_{n'}|]. \tag{23}$$

The range parameter α_h can be related to the tunneling probability that decreases exponentially with distance. In a first, rough adiabatic approximation the electrons are at any time in a local equilibrium distribution, we can estimate the distribution of the free electrons in the polarization potential field by a (classical) Boltzmann law. A full quantum mechanical description of the electrons in the field of the fast changing lattice is rather difficult. To simplify this situation we postulate that the electrons allow a Markov description. Thus we move from the *reversible* Schrödinger equation for the occupation numbers in the TBA model to an *irreversible* description by a Monte Carlo dynamics and the corresponding Pauli master equation [1,2]. The basic assumption is that the electrons follow a hopping dynamics with quantum mechanical probabilities for the transition from site n to site n' given by

$$W(n, n') = \frac{V_0^2}{\hbar} \exp[-2\alpha_h |\mathbf{r}_n - \mathbf{r}_{n'}|] E(n, n', \beta). \tag{24}$$

Here $E(n, n', \beta)$ is some symmetrical function which in the Pauli approximation is a delta function $E \sim \delta(E_n - E_{n'})$ [1,2]. Several other approximations are known which take into account the influence of the heat bath as e.g. the Lorentz profile. We use her as in references [3–5] a Monte Carlo approximation for the transition probabilities

$$E(n, n') = 1 \quad \text{if} \quad E_n < E_{n'}, \tag{25}$$

$$E(n, n') = \exp[-\beta(E_n - E_{n'})] \quad \text{if} \quad E_n > E_{n'}. \tag{26}$$

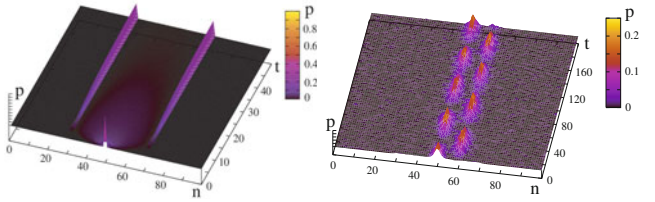

Fig. 4. (Color online) Evolution of the electron probability density for a 1d heated lattice ($N = 100$) with two energy wells at $T = 0.01$. Left panel: evolution according to the Pauli equation (27) of an initial electron distribution concentrated between two wells with depth $E_n = -2$ located at $n = 30$ and $n = 70$. The irreversible dynamics of the electron density leads to an equal distribution around potential wells (parameter of the transitions $\tau = 10$). Right panel: in the TBA-Schrödinger evolution the electron density is oscillatory with $\alpha_h = 0.1$, $V_0 = 0.1$, with the two wells separated by a distance 10 and with depths $E_n = -5$.

Then the Pauli master equation for the occupation probabilities of electrons p_n of the state n, given here by the position $\mathbf{r}_n$ with the energy E_n, is

$$\frac{dp_n}{dt} = \sum_{n'} [W_{nn'}p_{n'} - W_{n'n}p_n]. \qquad (27)$$

Since the detailed balance is obeyed, it is guaranteed that in thermal equilibrium an H-theorem is valid and any initial distribution tends to the *canonical* distribution, which is the target distribution of the master equation. Figure 4 illustrates results of our computer simulations with two fixed wells, depth 2 (in our units 2D), $n = 30$ and $n = 70$. We have considered two different initial conditions. In the first case the initial electron density is uniformly distributed. In the second case we initially have a delta-like distribution at position $n = 50$ in between both wells. We have seen that the relaxation to a *canonical* distribution with two peaks around the positions of energy wells is rather fast as in a few time units the final distribution is reached. Clearly the Pauli equation describes a basically different behavior from that of the Schrödinger equation. In the latter we have a *reversible* description and see a (quasi) periodic return to the initial state. In the Pauli description the *irreversible* behavior is due to the neglect of the off-diagonal terms of the density matrix. The coupling to a surrounding heat bath may be considered as the reason for the decay of off-diagonal elements. The quasiperiodicity in the Schrödinger picture leads to the oscillatory evolution (with an eventual small damping as shown in the right panel of Fig. 4). Indeed the TBA-Schrödinger dynamics includes coherent motions of the electron density between the two wells which is tunneling-like and leads to oscillations. The small damping results from the transfer of energy to the classical modes which are described by the irreversible Langevin equation. In the Pauli dynamics the coherence between the phases is destroyed thus leading to the irreversible approach to distributions concentrated around attracting potential wells. Note that in order to get control over the dynamics of electrons an irreversible

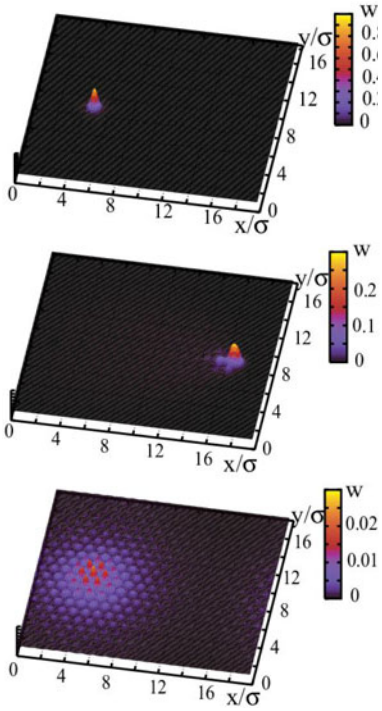

Fig. 5. (Color online) 2d Morse lattice. Soliton and electron initially placed at the same site in the same axis, x, subsequently travel together as a solectron along this same axis. Upper panel: initial distribution of the electron probability density. Center panel: time and space evolution according to Pauli equation (27) the density after $t = 3$ units for an electron interacting with an energetic soliton (the same excitation as in Fig. 1) moving along the crystallographic axis x. Bottom panel: quickly spreading corresponding electron distribution when the interaction with the lattice is switched off, $\alpha = 0$, as expected. Parameter values: $N = 400$, $b\sigma = 4$ and $T = 0.01$.

dynamics which is characteristic for macroscopic thermal systems may be of advantage. Interpreting these results in other words, the mechanisms of controlling we are studying here, would not work well at $T = 0$ due to the *reversibility* of quantum mechanics. Therefore our proposed electron control will work at moderate albeit high enough temperatures. For instance, $T = 0.01$ in our energy units corresponds to about 150 K.

Figure 5 illustrates that in probability density free electrons in a 2d lattice spread in rather short times over the whole accessible space. In the presence of solitons excited on the lattice in an appropriate way, a bound state is formed and the electron density is kept together and largely follows the soliton in a narrow region of space. We note that the shape of the bound state electron density as well as the compression density is similar to the lump solutions of the Kadomtsev-Petiashvili equation [25]; this needs further studies.

Further results on representations of electron probability densities are shown in Figures 6 and 7. We note that our electron – lattice dynamics is in a regime were the lattice nonlinearity dominates in comparison to self-trapping effects [26,27]. Further we note that the

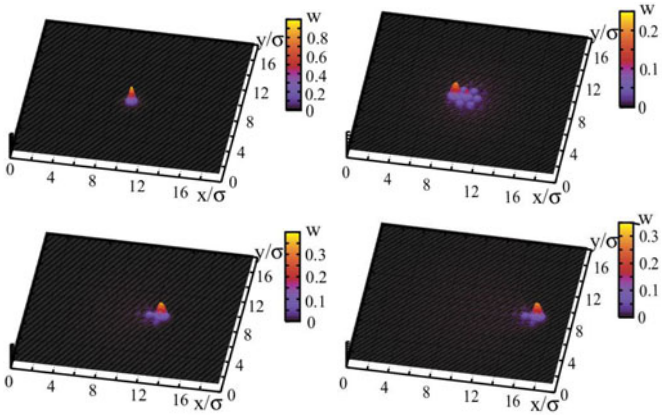

Fig. 6. (Color online) 2d Morse lattice. Soliton and electron initially placed at different sites in the same axis x (electron is placed at the center of the lattice and soliton slightly behind it) subsequently travel together as a solectron bound state along this same axis. The four pictures correspond to four successive time instants. Parameter values: $N = 400$, $b\sigma = 4$, $U_e = 0.1$, $A = 2$, $\kappa = 2.5$ and $T = 0.01$.

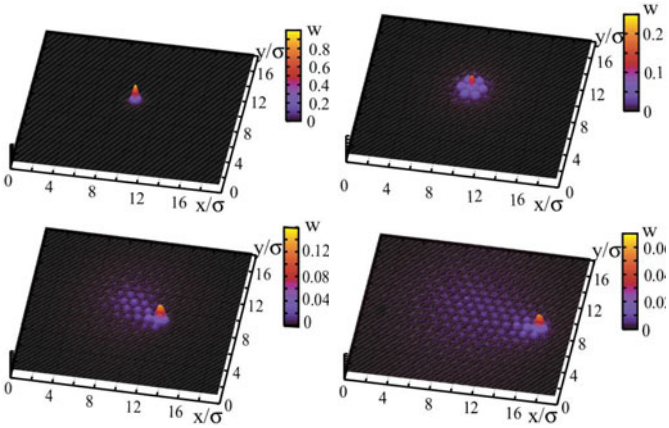

Fig. 7. (Color online) 2d Morse lattice. Soliton and electron placed near to each other but at different rows. The traveling soliton along the crystallographic axis, x, interacts with the electron being able to gather the electron probability density around itself, in kind of "vacuum cleaning" process [8], eventually forming a solectron bound state and hence bringing the electron to the boundary of the lattice. The four pictures correspond to successive time instants. Parameter values: $N = 400$, $b\sigma = 4$, $U_e = 0.1$, $A = 2$, $\kappa = 2.5$ and $T = 0.01$.

supersonic lattice polarons which are essentially due to the lattice nonlinearities are more stable against perturbations than the subsonic polarons [26,27].

4 Discussion

We have developed theoretical tools for the study of *slaved* or otherwise said, *controlled*, individual electron evolution by means of lattice soliton-like excitations acting as carriers along the crystallographic axes of a e.g. a triangular lattice. For each crystallographic axis there exist two relatively stable electron-soliton bound states (solectrons) corresponding to the two possible directions of motion. Our computer simulations use Langevin equations for atoms with Morse interactions and quantum kinetic equations of Pauli-type for the electron evolution. We have shown that with appropriate initial conditions, e.g. by a sudden increase of the momentum of one atom, the above mentioned bound states can be created able to carry electrons at near-to-sound velocity over a distance of a few hundred sites with no significant loss of electron density and momentum. This appears as a clear case of electron surfing. In the electron trapping process which we study, the local lattice compressions significantly deform the potential landscape acting on added, excess electrons and create a moving *guiding* well or trap. There is also a feedback of the concentration of electron density on the lattice deformation which we have neglected in a first approximation. Indeed, in the supersonic case, for the given parameter values, this feedback is rather small, changing the results by less than a few percent. Generally, the electrons tend to be trapped in the regions of maximal density of lattice points created by the local compressions and then forced to move dynamically bound to the soliton-like compressions which in 2d is favored along the crystallographic axes. This surfing effect is offering a novel way of controlling and transporting electrons.

Save the scale, our results seem to agree well with findings reported long ago by Donovan and Wilson [30,31] in experiments with polydiacetylene (PDA) and other derivatives. PDA can form perfect single crystals, in which the polymer lattice rows are straight and parallel over macroscopic (mm) distances. A conjugated π electron system forms a semiconducting band system along the carbon backbone. The polymer side groups are large, and the carbon backbones on adjacent chains are a long distance apart, ca. 0.7 nm, so there is negligible overlap between the π electron wave functions of adjacent chains. In the experiments of Donovan and Wilson photo created carriers were found to travel at room temperature at a field-independent constant velocity, over several decades of the applied field. The electron velocity of 2 km/s, was subsonic as the estimated sound velocity was 3.6 km/s. Other results with crystals in which the TS group was replaced by DCH, denoted PDADCH, provided supersonic velocities of ca. 5 km/s [32]. Such free ride of the electron was observed over mm before electron was trapped at a defect. Wilson [33] argued that an electron in 1d, described in the TBA, interacts via a deformation potential, with the acoustic distortion of the harmonic 1d lattice. This resulted in a large polaron, comprising an electron localized in the deformation which it has caused. This theory was further developed by Gogolin [34,35]. In both cases theory allows subsonic motions only. At variance to the theoretical interpretation given by Wilson and Gogolin our view is that *anharmonic* lattice oscillations leading to our solectron may be a better suited interpretation as we predict subsonic as well as supersonic electron motions.

Let us conclude by commenting on some recent experiments on electron *surfing* between quantum dots, a mm apart, [36,37] using linear, highly monochromatic, harmonic surface acoustic waves (SAW) [38,39] as carriers along a piezoelectric GaAs layer. A kind of ping-pong behavior was also reported between the entry and exit gates. Due to experimental measurement constraints the temperature was quite low (20 mK and 300 mK, respectively).

Linear and nonlinear SAW propagating in a homogeneous elastic medium, piezoelectric, or otherwise, exhibit no dispersion. If the medium is nonlinear, as e.g. in *anharmonic* crystal lattices, an initial sinusoidal SAW can create higher harmonics which may grow without being inhibited by dispersion. Dispersion can be introduced by coating the medium with a thin film of another material with elastic and structural/mechanical properties different from those of the substrate. On the other hand, by an appropriate choice of the film thickness, the effects of *nonlinearity* and *dispersion* can balance each other thus sustaining solitons. Long ago Nayanov [40,41] was able to observe, at room temperature, solitons (solitary and cnoidal waves) on $LiNbO_3$ layers covered by an SiO film (obtained by evaporation) of appropriate thickness. Electron surfing with solitons at this *macroscopic* scale is yet to be observed. Yet as high amplitude SAW tend to deform to sawtooh shape and eventually break, the suggestion coming from our theory is that for electron surfing, no matter the scale involved, solitons shoud be better carriers than linear waves, even if highly monochromatic.

The authors acknowledge fruitful discussions and correspondence with L. Brizhik, E. Brändas, L. Cisneros, L. Cruzeiro, F. de Moura, J. Feder, D. Hennig, R. Lima, and G. Röpke. They also wish to thank R.P.G. McNeil and T. Meunier for sharing with us their electron surfing experiments in piezoelectric GaAs layers and V.I. Nayanov for his enlighting description of soliton SAW in nonlinearly elastic, piezoelectric $LiNbO_3$ layers where wave dispersion able to balance nonlinearity of the substrate is monitored by depositing, via evaporation, SiO films of suitable thickness. E.G. Wilson is also gratefully acknowledged for detailed information on his experiments on soliton-mediated charge motion in PDA crystals. This research was supported by the Spanish *Ministerio de Economía y Competitividad*, under Grant MAT2011-26221.

References

1. W. Pauli, *Festschrift zum 60. Geburtstage A. Sommerfelds* (S. Hirzel, Leipzig, 1928), p. 30
2. R. Tolman, *The Principles of Statistical Mechanics* (Oxford University Press, Oxford, 1938), Sects. 100, 102, 105
3. A.P. Chetverikov, W. Ebeling, M.G. Velarde, Eur. Phys. J. B **70**, 117 (2009)
4. A.P. Chetverikov, W. Ebeling, M.G. Velarde, Eur. Phys. J. B **80**, 137 (2011)
5. A.P. Chetverikov, W. Ebeling, G. Röpke, M.G. Velarde, Contr. Plasma Phys. **51**, 814 (2011)
6. P. Morse, Phys. Rev. **34**, 57 (1929)
7. D. Hennig, A. Neissner, M.G. Velarde, W. Ebeling, Phys. Rev. E **76**, 046602 (2007)
8. M.G. Velarde, W. Ebeling, A.P. Chetverikov, D. Hennig, Int. J. Bifur. Chaos **18**, 521 (2008)
9. M.G. Velarde, W. Ebeling, A.P. Chetverikov, Int. J. Bifur. Chaos **18**, 3815 (2008)
10. M.G. Velarde, A.P. Chetverikov, W. Ebeling, D. Hennig, J. Kozak, Int. J. Bifur. Chaos **20**, 185 (2010)
11. L.D. Landau, Phys. Z. Sowjetunion **3**, 664 (1933)
12. S.I. Pekar, *Untersuchungen über die Elektronentheorie* (Akademie Verlag, Berlin, 1954), and references therein.
13. M.G. Velarde, J. Comput. Appl. Maths **233**, 1432 (2010)
14. O.G. Cantu Ros, L. Cruzeiro, M.G. Velarde, W. Ebeling, Eur. Phys. J. B **80**, 545 (2011)
15. Y.A. Omarbakieva, C. Fortmann, T.S. Ramazanov, G. Röpke, Phys. Rev. E **82**, 026407 (2010)
16. F. Marchesoni, C. Lucheroni, Phys. Rev. E **44**, 5303 (1991)
17. M. Toda, *Nonlinear Waves and Solitons* (KTK Scientific Publishers, Tokyo, 1989)
18. M. Toda, *Theory of Nonlinear Lattices*, 2nd edn. (Springer-Verlag, New York, 1989)
19. J. Dancz, S.A. Rice, J. Chem. Phys. **67**, 1418 (1977)
20. T.J. Rolfe, S.A. Rice, J. Dancz, J. Chem. Phys. **70**, 26 (1979)
21. A.P. Chetverikov, W. Ebeling, M.G. Velarde, Physica D **240**, 1954 (2011)
22. A.P. Chetverikov, W. Ebeling, M.G. Velarde, Wave Motion **48**, 753 (2011)
23. M. Remoissenet, *Waves Called Solitons Concepts and Experiments* (Springer, Berlin, 2010)
24. A.P. Chetverikov, W. Ebeling, M.G. Velarde, Eur. Phys. J. B **51**, 87 (2006)
25. A.A. Minzoni, N.F. Smyth, Wave Motion **24**, 291 (1996)
26. A.S. Davydov, *Solitons in Molecular Systems*, 2nd edn. (Reidel, Dordrecht, 1991)
27. A.V. Zolotaryuk, K.H. Spatschek, A.V. Savin, Phys. Rev. B **54**, 266 (1996)
28. H. Böttger, V.V. Bryksin, *Hopping Conduction in Solids* (Akademie-Verlag, Berlin, 1985)
29. J.C. Slater, *Quantum Theory of Molecular and Solids. The Self-Consistent Field for Molecules and Solids* (McGraw-Hill, New York, 1974), Vol. 4
30. K.J. Donovan, E.G. Wilson, Philos. Mag. B **44**, 9 (1981)
31. K.J. Donovan, E.G. Wilson, Philos. Mag. B **44**, 31 (1981)
32. K.J. Donovan, P.D. Freeman, E.G. Wilson, J. Phys. C **18**, L275 (1985)
33. E.G. Wilson, J. Phys. C, Sol. Stat. Phys. **16**, 6739 (1983)
34. A.A. Gogolin, JETP Lett. **8**, 511 (1986)
35. A.A. Gogolin, Phys. Rep. **157**, 348 (1988)
36. S. Hermelin, S. Takada, M. Yamamoto, S. Tarucha, A.D. Wieck, L. Saminadayar, C. Bäuerle, T. Meunier, Nature **477**, 435 (2011)
37. R.P.G. McNeil, M. Kataoka, C.J.B. Ford, C.H.W. Barnes, D. Anderson, G.A.C. Jones, I. Farrer, D.A. Ritchie, Nature **477**, 439 (2011)
38. A.P. Mayer, Phys. Rep. **256**, 237 (1995), and references therein
39. A.P. Mayer, Ultrasonics **48**, 478 (2008)
40. V.I. Nayanov, I.A. Vasil'ev, Sov. Phys. Solid State **25**, 1430 (1983)
41. V.I. Nayanov, JETP Phys. Lett. **44**, 314 (1986)